RESEARCH ARTICLE

CATALYSIS

Univariate classification of phosphine ligation state and reactivity in cross-coupling catalysis

Samuel H. Newman-Stonebraker[1]†‡, Sleight R. Smith[2]†, Julia E. Borowski[1], Ellyn Peters[2], Tobias Gensch[2]§, Heather C. Johnson[3]¶, Matthew S. Sigman[2]*, Abigail G. Doyle[1]*‡

Chemists often use statistical analysis of reaction data with molecular descriptors to identify structure-reactivity relationships, which can enable prediction and mechanistic understanding. In this study, we developed a broadly applicable and quantitative classification workflow that identifies reactivity cliffs in 11 Ni- and Pd-catalyzed cross-coupling datasets using monodentate phosphine ligands. A distinctive ligand steric descriptor, minimum percent buried volume [%V_{bur} (min)], is found to divide these datasets into active and inactive regions at a similar threshold value. Organometallic studies demonstrate that this threshold corresponds to the binary outcome of bisligated versus monoligated metal and that %V_{bur} (min) is a physically meaningful and predictive representation of ligand structure in catalysis.

Chemists commonly use data-driven modeling to understand the many complex relationships connecting chemical structure to reactivity (*1*, *2*). For many reactions, a continuous dependence is observed between a descriptor—a mathematical way to describe a subunit or the entirety of a molecule—and chemical reactivity, as captured by linear free-energy relationships (*3*, *4*). However, some processes exhibit reactivity cliffs, wherein a criterion or threshold value of a given descriptor must be met for the reaction to occur (i.e., a binary response) (*5*). Identification of the molecular feature that is mechanistically linked to a reactivity cliff could enable the classification of molecules by structure, predict reaction outcomes for unseen examples, and reveal key mechanistic insights.

Transition metal–catalyzed cross-coupling represents a relevant case study for identifying reactivity cliffs. This reaction class is synthetically important because of its widespread use in the synthesis of pharmaceuticals (*6*) and materials (*7*). In addition, the success of these reactions is highly dependent on ancillary ligand identity, with monodentate phosphines among the most frequently used (*8*, *9*) (Fig. 1A). Given that thousands of unique structural examples exist, chemists have developed numerous tools to quantitatively describe the diverse steric and electronic properties of monodentate phosphines (*10*). These descriptors—including Tolman cone angle (*11*, *12*), solid angle (*13*), Sterimol (*14*), and percent buried volume (%V_{bur}) (*15*–*17*) (Fig. 1B)—have been used to correlate structure-reactivity trends in cross-coupling datasets (*2*, *18*). However, there are situations in which seemingly similar ligands afford substantially different reactivities (*19*), suggesting the presence of discontinuities in ligand reactivity (*20*).

Considering this, we hypothesized that these discontinuities were evidence of reactivity cliffs and linked to a phosphine structural feature yet to be defined. Identification of such a descriptor would not only allow for the development of a statistical means to classify active and inactive ligands but also provide a quantitative tool for mechanistically rationalizing ligand performance. Herein, we provide a workflow and analysis to achieve these goals. Using the organophosphorus(III) descriptor library recently developed by Gensch *et al.* (*kraken*) that possesses nearly 200 conformationally representative descriptors for each of several thousand monodentate phosphines (*21*) (Fig. 1C), we were able to classify 11 Ni- and Pd-catalyzed cross-coupling datasets into active and inactive regions of reactivity based on whether the metal preferentially coordinates to one or two phosphines (i.e., catalyst ligation state). Spectroscopic and crystallographic organometallic studies demonstrate that minimum percent buried volume [%V_{bur} (min)] is the single descriptor able to achieve this classification. Although %V_{bur} describes the steric bulk of any given ligand structure within 3.5 Å of the metal center, %V_{bur} (min), a previously unexplored variant of the descriptor, quantifies the smallest %V_{bur} among all of the ligand's energetically accessible conformers. Ultimately, this analysis revealed nonintuitive trends in organometallic chemistry and can thereby serve as an important mechanistic tool to understand and predict monodentate phosphine structure-reactivity relationships and catalyst ligation state in cross-coupling catalysis (Fig. 1D).

[1]Department of Chemistry, Princeton University, Princeton, NJ 08544, USA. [2]Department of Chemistry, University of Utah, Salt Lake City, UT 84112, USA. [3]Process Research and Development, Merck & Co., Inc., Rahway, NJ 07065, USA.
***Corresponding author. Email: sigman@chem.utah.edu (M.S.S.); agdoyle@chem.ucla.edu (A.G.D.)**
†These authors contributed equally to this work.
‡Present address: Department of Chemistry and Biochemistry, University of California, Los Angeles, CA 90095, USA.
§Present address: Department of Chemistry, TU Berlin, 10623 Berlin, Germany.
¶Present address: Drug Substance Technologies, Process Development, Amgen, Inc., Cambridge, MA 02142, USA.

Exploration of phosphine steric descriptors in Ni catalysis

Our initial platform for probing the presence of ligand reactivity cliffs was inspired by a recent study from the Doyle group that identified a new class of monodentate phosphine ligands—the DinoPhos ligands [TriceraPhos and TyrannoPhos (Fig. 1A)]—as distinctively effective for the Ni-catalyzed cross-coupling of acetals with aryl boroxines (*19*). The characteristic that distinguished the DinoPhos ligands from those that were less successful in the reaction was found to be their high level of remote steric bulk, quantified by both a large cone angle and small %V_{bur} value. The large cone angles of the DinoPhos ligands suggested that they may behave like the sterically bulky phosphines developed for Pd-catalyzed cross-couplings [e.g., P(*t*-Bu)$_3$ or CyJohnPhos (*t*-Bu, *tert*-butyl; Cy, cyclohexyl); Fig. 1A], where preferential formation of monoligated (denoted as L_1) Pd complexes has been shown to be critical for reaction success (*22*–*26*). However, the small %V_{bur} characterized these ligands as similar to smaller structures [e.g., PPh$_3$ (Ph, phenyl); Fig. 1A] that tend to form bisligated (denoted as L_2) complexes. The observation that this distinctive steric profile was essential for reaction success in Ni catalysis raised questions about its impact on catalyst ligation state and prompted us to use Ni-catalyzed cross-coupling reactions as a case study for the identification of ligand reactivity cliffs.

The original study by the Doyle lab included 19 phosphines, which we supplemented with 15 additional ligands to span the entire range of %V_{bur} (reaction I; Fig. 2A). We also collected data on Ni-catalyzed Csp^2–Csp^2 Suzuki-Miyaura coupling (SMC) reactions with aryl chlorides using high-throughput experimentation. The ligand set was assembled from a combined Doyle and Merck Sharp & Dohme inventory to encompass 90 monodentate phosphines that are included in the *kraken* virtual library (*21*), with *k*-means clustering applied to enable a selection of structures that broadly covered phosphine chemical space (*27*). These ligands were evaluated for four cross-coupling reactions wherein the aryl halide and aryl boronic acid were altered (reactions II to V; Fig. 2A). The coupling partners included a range of electronic and steric features that could affect different aspects of the elementary steps of the catalytic cycle. Notably, the DinoPhos ligands were among the highest yielding in each of these reactions, along with DrewPhos (*28*), a triarylphosphine ligand that possesses *t*-Bu groups at the remote 3,5 positions of the arenes, similar to the DinoPhos ligands.

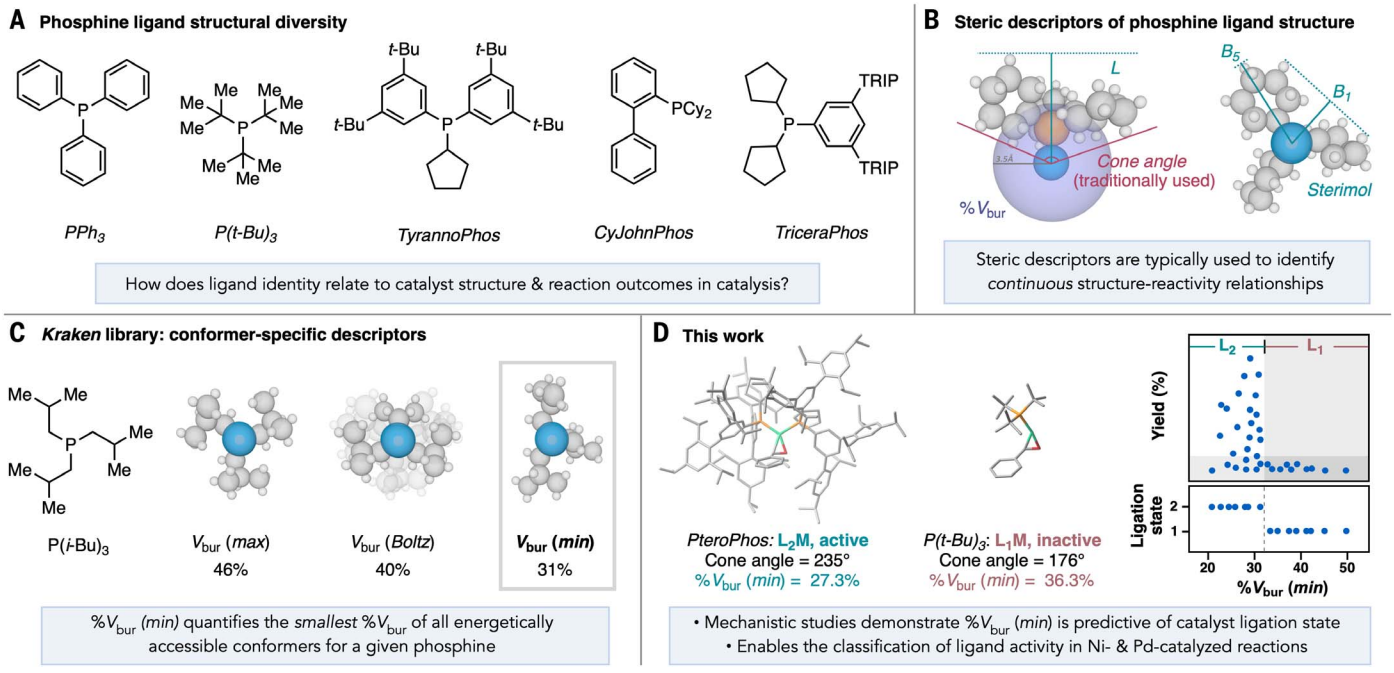

Fig. 1. Studying phosphine ligand reactivity using structural descriptors. (**A**) Examples of monodentate phosphines used in Ni and Pd cross-coupling reactions, including TyrannoPhos and TriceraPhos (DinoPhos ligands) recently reported by the Doyle lab (*19*). TRIP, 2,4,6-triisopropylphenyl. (**B**) Commonly used methods for quantifying phosphine steric properties. Cone angle is the traditionally used descriptor for quantifying monodentate phosphine steric bulk and is defined as the angular width (in degrees) of an imaginary cone needed to encapsulate the entire phosphine structure; the vertex of the cone is defined by a metal atom bound to the ligand with a bond length of 2.28 Å. $\%V_{bur}$, a more modern descriptor designed initially to study N-heterocyclic carbenes, is defined as the volume percent of the phosphine's atoms that fill an imaginary sphere of 3.5 Å radius that is centered on a metal atom bound to the phosphine with a bond length of 2.28 Å. Sterimol descriptors B1 and B5 describe the lowest and highest width of the ligand perpendicular to the metal-phosphorus axis, respectively, and Sterimol L describes the ligand's length along that axis. (**C**) Phosphine descriptor library (*kraken*) capturing multiple ligand conformers, with maximum, Boltzmann average, and minimum $\%V_{bur}$ values of the conformational ensemble of P(*i*-Bu)$_3$ shown. (**D**) This work. L1, one equivalent of ligand bound to metal; L2, two equivalents of ligand bound to metal; M, metal.

With these data, we sought to determine how the *kraken* steric descriptors relate to reaction performance. For each reaction, the yield was evaluated against representative descriptors in the library; as three examples, the cone angle (*29*), Boltzmann averaged $\%V_{bur}$ of the ligand's conformational ensemble [$\%V_{bur}$ (Boltz)], and $\%V_{bur}$ of the library conformer with the smallest buried volume [$\%V_{bur}$ (min)] are shown in Fig. 2B. Whereas the cone angle descriptors did not provide clear reactivity cutoffs, both $\%V_{bur}$ (Boltz) and $\%V_{bur}$ (min) allowed for classification of ligand performance into "active" and "inactive" bins (details of the classification tool will be described below for quantitative demarcation of the thresholds), though several outliers were present with the former. The $\%V_{bur}$ (min) descriptor revealed sharp cutoffs in reactivity, wherein nearly all ligands above 32% were found to be unreactive. Ligands that were unsuccessful at promoting reactivity below 32% V_{bur} (min) were grouped in their own bin, wherein electronic features and catalyst-poisoning functionality (e.g., cyano, carbonyl, and halide groups) appeared to be largely responsible for their inactivity. The use of $\%V_{bur}$ (min), but not $\%V_{bur}$ (Boltz), allowed for various highly flexible scaffolds such as P(*i*-Bu)$_3$, PBn$_3$, and small (dialkyl)-*ortho*-biaryl (Buchwald-type) phosphines (*23*, *30*, *31*), to be successfully classified (*i*-Bu, isobutyl; Bn, benzyl). Thus, this steric descriptor best categorized phosphines into active and inactive bins (tables S15 and S16), with a reactivity threshold of ~32% V_{bur} (min) appearing across all reactions studied.

Mechanistic origin of $\%V_{bur}$ (min) reactivity thresholds

The presence of reaction-independent reactivity cliffs relative to $\%V_{bur}$ (min) in these data prompted us to investigate the mechanistic basis for this descriptor's importance. Given the importance of ligation state in cross-coupling catalysis, we questioned whether this descriptor is predictive of the preference for forming L_2M versus L_1M complexes (M, metal). Historically, the development of large ligands—intuitively captured through the cone angle descriptor—is an established principle to favor L_1M and thereby promote reactivity in Pd catalysis (*22*–*26*). Although TriceraPhos and TyrannoPhos both have cone angle values higher than many phosphines known to form L_1 species, $\%V_{bur}$ (min) categorizes their reactivity with those that form L_2 Ni and Pd complexes (*22*, *32*). Thus, this interpretation of the observed reactivity cliffs would suggest that steric bulk within the metal's first coordination sphere primarily governs the ligation state outcome, regardless of the overall size of the phosphine.

To interrogate this hypothesis, we surveyed a subset (28 phosphines) of the ligands used across the Ni-catalyzed SMC reactions to determine ligation state spectroscopically. L_nNi(4-fluorobenzaldehyde) was chosen as a platform, because its three nuclear magnetic resonance (NMR) handles (^{1}H, ^{19}F, and ^{31}P) provided a readout of the in situ ligation state at the metal center (figs. S4 to S87) upon reaction of Ni(COD)$_2$ (COD, 1,5-cyclooctadiene) with the aldehyde and two equivalents of phosphine (reaction VI; Fig. 3A) (*33*, *34*). Each ligand was assigned as forming L_2Ni or L_1Ni complexes based on the observed spectra. The results of these experiments were then evaluated with steric features from the library to determine which ones classified the ligands into regions of similar ligation states (Fig. 3B; see fig. S3 for additional descriptors). As observed with the cross-coupling reaction yields, cone angle was unable to partition the ligands. Indeed, the DinoPhos ligands and DrewPhos all formed L_2Ni complexes exclusively, despite having

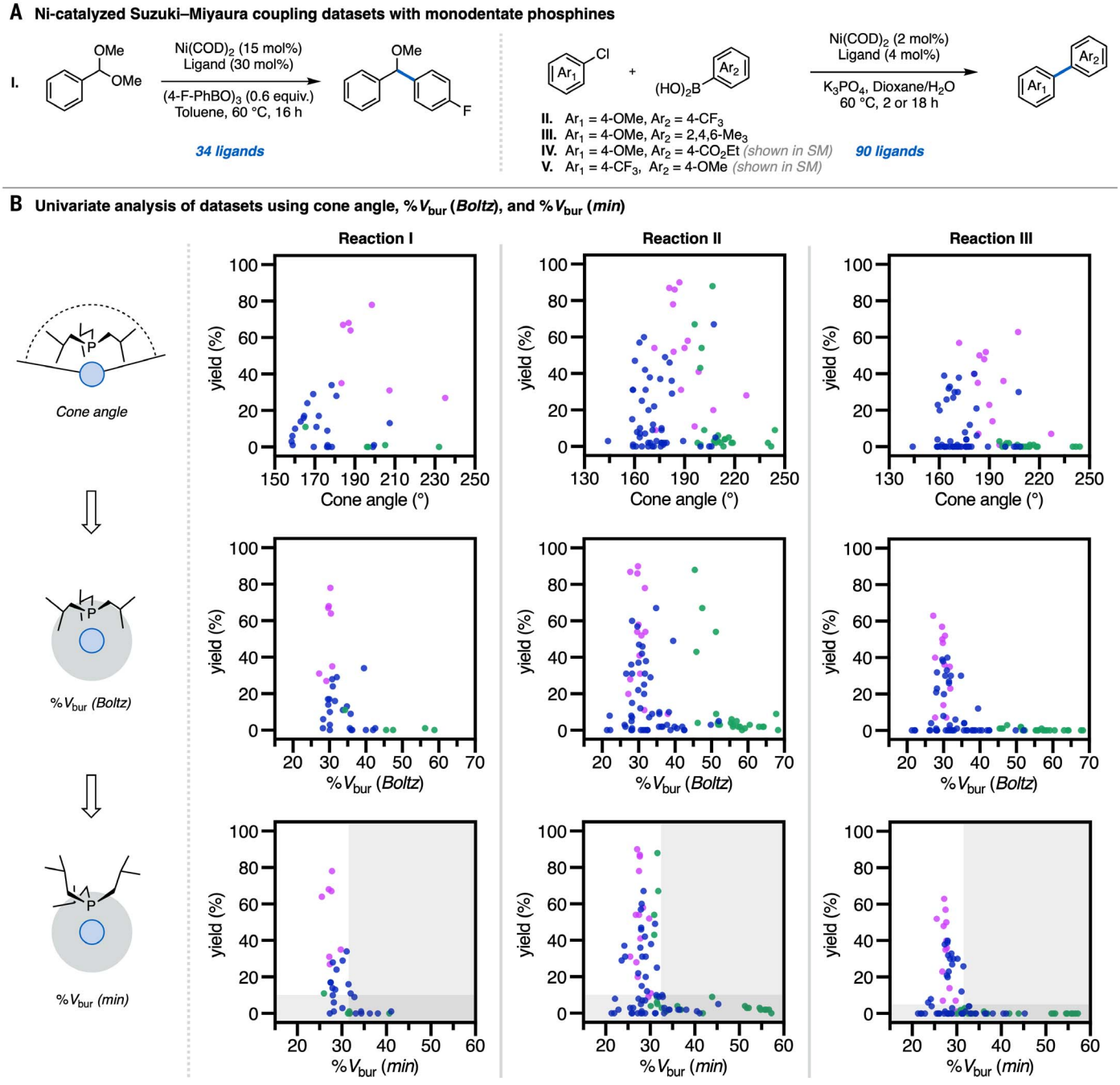

Fig. 2. Investigation of phosphine steric parameters in Ni-catalysis datasets. (**A**) Ni-catalyzed Suzuki-Miyaura datasets collected with monodentate phosphine ligands, including the DinoPhos ligands. Ar, aryl; Et, ethyl. (**B**) Analysis of datasets with the steric parameters cone angle, %V_{bur} (Boltz), and %V_{bur} (min). Pink dots represent DinoPhos-type ligands, green dots represent Buchwald-type (dialky)-*ortho*-biaryl ligands, and blue dots represent all others.

some of the largest cone angle values among ligands evaluated. The %V_{bur} (Boltz) descriptor correctly grouped the DinoPhos-type ligands with other L_2Ni-forming phosphines; however, some flexible ligands [MeJohnPhos, P(*i*-Bu)$_3$, and PBn$_3$; Me, methyl] remained misclassified with L_1Ni-forming ligands. Similar to the catalytic reactions, %V_{bur} (min) resolved these outliers and resulted in a sharp cutoff just below 32% between the L_2Ni and L_1Ni regimes. This value closely matched the reactivity thresholds observed in reactions I to V.

Given this finding, we hypothesized that we could predict the ligation state of new ligands, enabling a prescreening of structures that may be challenging to access synthetically. To test this, we conceptualized a new DinoPhos ligand, PteroPhos, which possesses two aryl groups with 2,4,6-triisopropylphenyl (TRIP) substituents at the 3,5 positions (Fig. 4A). Its computed cone angle is 235°, one of the largest among all monodentate phosphines studied. Despite the enormous size of this ligand, as ascertained by visual inspection, and its cone-angle value, its relatively low %V_{bur} (min) of only 27.2% suggested that PteroPhos should form L_2Ni complexes and be effective in Ni-catalyzed SMCs. Indeed, upon preparation of this ligand, we found that it formed a L_2Ni(4-fluorobenzaldehyde) complex (Fig. 3B) and

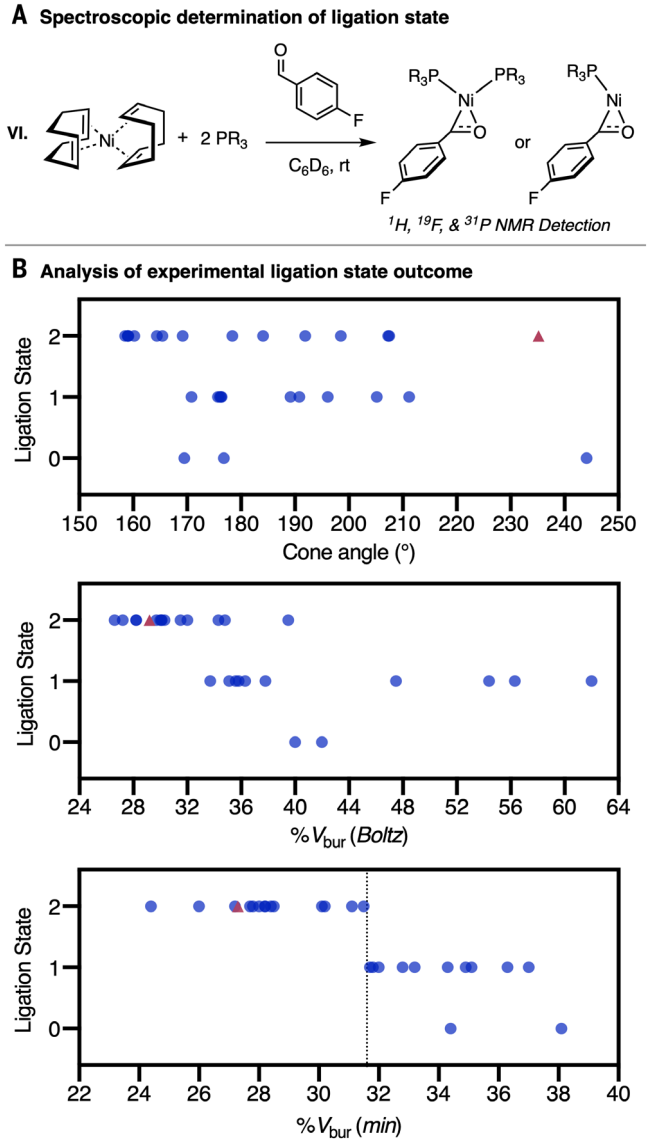

Fig. 3. Ligation state studies. (**A**) Reaction of $Ni(COD)_2$, 4-fluorobenzaldehyde, and two equivalents of phosphine for spectroscopic determination of ligation state using ^{1}H, ^{19}F, and ^{31}P NMR spectroscopy in C_6D_6 (25°C). R, variable substituent; rt, room temperature. (**B**) Ligation state experiments plotted against cone angle, $\%V_{bur}$ (Boltz), and $\%V_{bur}$ (min). The red triangle represents PteroPhos; blue dots represent all other phosphines studied. The (*t*-Bu)BrettPhos (nonligating) datapoint is beyond the *x*-axis range for the $\%V_{bur}$ (min) and $\%V_{bur}$ (Boltz) plots. See table S3 for conversion data for complexes. All ligands assigned as L_1Ni or L_2Ni had conversions >50% except for L_1Ni-forming PhP(*t*-Bu)$_2$ (39%) and P(*t*-Bu)$_3$ (17%). The vertical dotted line represents the location of the $\%V_{bur}$ (min) reactivity cliff.

was moderately active in Ni-catalyzed reactions I to V, consistent with the $\%V_{bur}$ (min) classification analysis.

We then sought to understand the structural importance of $\%V_{bur}$ (min) through crystallographic and computational studies (complexes **1** to **4**; Fig. 4A), to first rationalize why cone angle is not predictive of ligation state. Although our attempts at crystallizing L_2Ni(benzaldehyde) complexes bearing the DinoPhos ligands were not successful, we were able to obtain x-ray diffraction–quality crystals of $(DrewPhos)_2Ni$(2-naphthaldehyde) (**3**; Fig. 4A). As observed in the solid state, the two phosphines are positioned 116° cis to each other on the complex; because DrewPhos possesses a cone angle of 207°, a literal interpretation of cone angle as a description of phosphine size would suggest that there is 90° overlap of two solids, giving rise to considerable steric repulsion or distortion. Yet, when compared with the x-ray structure of $(PPh_3)_2Ni$(2-naphthaldehyde) (**1**; Fig. 4A), the two complexes exhibit very similar Ni–P bond lengths and P–Ni–P "bite angles," despite DrewPhos having a cone angle 48° larger than PPh_3. What cone angle does not capture is the nonuniform topology of the ligand structure distal to the metal. These less dense and more conformationally flexible regions can be arranged in a manner that accommodates a second ligand and/or substrate within the "cone," a recognized limitation that has led to the development of alternative steric descriptors (*12*, *15*, *17*, *35*). On this basis, cone angle is unsuccessful at classifying the ligation state and reactivity of the phosphines under study. Indeed, when compared with that of L_1 [P(*t*-Bu)$_3$]Ni(benzaldehyde) (**2**; Fig. 4A), the density functional theory (DFT)–optimized structure of $(PteroPhos)_2Ni$(benzaldehyde) (**4**; Fig. 4A) provides the most notable example of L_2 complexation being agnostic to substantial remote steric bulk.

Although this case study highlights the dependence of ligation state on steric bulk within the first coordination sphere, which is captured by the $\%V_{bur}$ descriptors, the ligands investigated in Fig. 4A had small variations between their $\%V_{bur}$ (min) and $\%V_{bur}$ (Boltz) values. To better understand the structural importance of $\%V_{bur}$ (min) in the classification of the catalytic (Fig. 2B) and ligation state experiments (Fig. 3B), the L_2Ni-forming ligand with the greatest difference between $\%V_{bur}$ (min) and $\%V_{bur}$ (Boltz) values, P(*i*-Bu)$_3$, was investigated. For this phosphine, the $\%V_{bur}$ values of the lowest-energy conformer and the Boltzmann-weighted average of all conformers (38.7 and 39.5%, respectively) are both substantially higher than those for other L_2Ni-forming ligands, and even higher than the $\%V_{bur}$ (Boltz) of L_1Ni-forming P(*t*-Bu)$_3$ (36.3%). However, an x-ray crystal structure of $[P(i\text{-}Bu)_3]_2Ni$(2-naphthaldehyde) (**5**; Fig. 4B) confirmed that two phosphines were bound to Ni, with $\%V_{bur}$ values determined to be 29.0 and 32.2%, nearly matching that of $\%V_{bur}$ (min) (31.1%). This analysis highlights that $\%V_{bur}$ (min) is a better representation of a phosphine when two equivalents are bound to a metal center. It suggests that the energetic benefit of coordinating a second phosphine to the metal outweighs the energetic cost of that phosphine assuming a conformation with a smaller buried volume below ~32%.

Finally, given the sharp catalytic and ligation state reactivity cliffs, we postulated that there would be a strong dependence on the thermodynamics of phosphine dissociation from L_2Ni(benzaldehyde) complexes with $\%V_{bur}$ (min). Out of all 28 phosphines studied in Fig. 3, only one [Cy_2P(*t*-Bu)] was found to have any spectroscopically observable equilibrium between L_2Ni and L_1Ni (1:4 L_2:L_1), with a $\%V_{bur}$ (min) value of 32.0% near the ligation state cutoff. Using Cy_2P(*t*-Bu) as a reference, the free energy of ligand dissociation (ΔG_{dissoc}) was calculated for 20 L_2Ni(benzaldehyde) complexes using DFT (Fig. 4C). [ΔG_{dissoc} was not found to be dependent on electronics in these

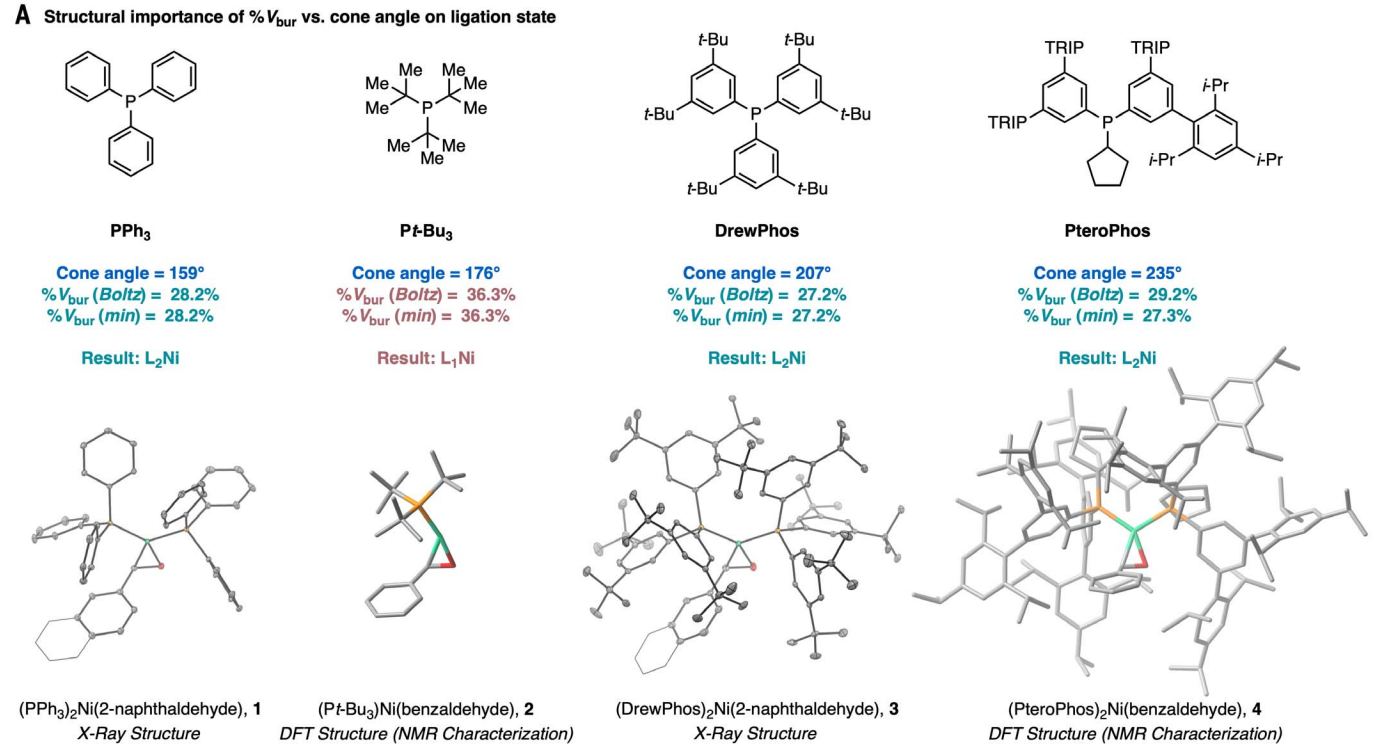

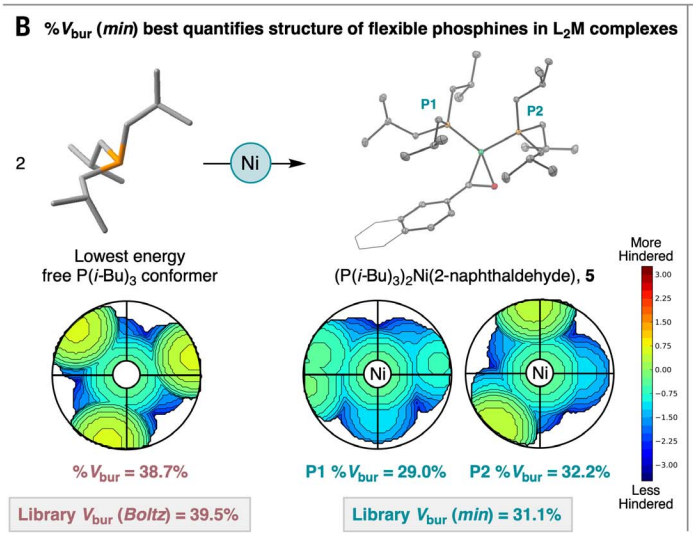

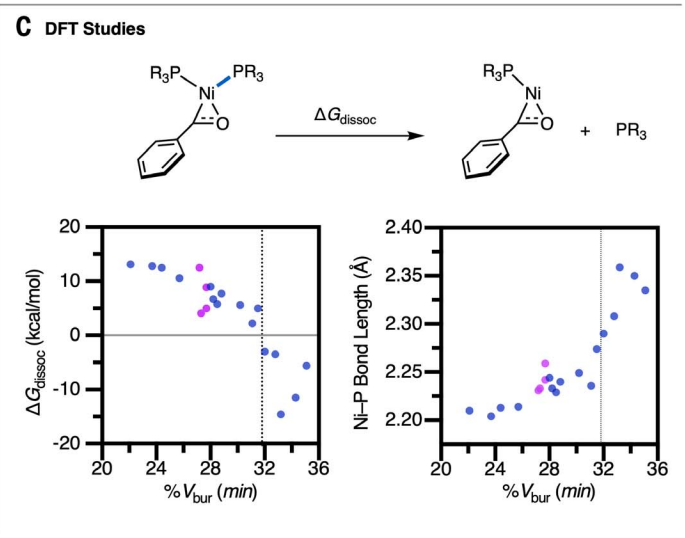

Fig. 4. Mechanistic studies of %V_{bur} (min) ligation state threshold. (**A**) Ligands with large cone angles, but relatively small %V_{bur} values, can form L_2Ni, supported by experimentally characterized solid-state structures [Oak Ridge thermal ellipsoid plot (ORTEP) with 30% thermal ellipsoids is shown; hydrogens are omitted for clarity] of $(PPh_3)_2Ni$(2-naphthaldehyde) and $(DrewPhos)_2Ni$(2-naphthaldehyde), along with DFT-simulated structures of $[P(t\text{-}Bu)_3]Ni$(benzaldehyde) and $(PteroPhos)_2Ni$(benzaldehyde) optimized at the B3LYP-D3/6-31G(d,p)[SDD] level of theory. Pr, propyl. (**B**) Formation of $[P(i\text{-}Bu)_3]_2Ni$(2-naphthaldehyde) (ORTEP is as above). The %V_{bur} values of the ligands in the crystal structure are in agreement with the corresponding library value of %V_{bur} (min). Steric heat maps of the phosphine ligands are shown, looking down the Ni–P bond. (**C**) DFT-calculated dissociation energies and bond lengths for L_2Ni(benzaldehyde) complexes. Ni–P bond length was calculated from the highlighted bond. DinoPhos-type ligands (including DrewPhos) are highlighted in pink. Calculations performed at M11-L/def2-TZVP|SMD(benzene)//B3LYP-D3/6-31G(d,p)[SDD]|SMD(benzene) level of theory.

studies; see supplementary materials (SM) for details.] A %V_{bur} (min) cutoff of 32% cleanly separated the regions of positive and negative ΔG_{dissoc}, with the remote steric bulk of the DinoPhos ligands and DrewPhos having minimal impacts on dissociation energy. Furthermore, the sharp downtick in the ΔG_{dissoc} values as the %V_{bur} (min) of the phosphine approached 32% corresponded with a substantial uptick in the Ni–P bond length of the computed L_2 complex, a reflection of the increased steric pressure caused by filling Ni's first coordination sphere at this value. Together, these studies demonstrate the physical significance of the %V_{bur} (min) descriptor and the 32% threshold value observed experimentally.

Development of a threshold analysis algorithm

With the identification of sharp reactivity cliffs in Ni SMC datasets, we sought to formalize the analysis to aid in the automated discovery

of thresholds and consequent classification of ligands within a diverse array of reaction datasets. Although $\%V_{bur}$ (min) was the most successful descriptor in classifying ligands in the Ni-catalyzed cross-coupling reactions, the workflow was designed to use all available descriptors and was implemented as follows: The user first defines the percent yield or selectivity for a "successful" reaction (either above "ligand-less" control reactivity or a single catalyst turnover), after which the data are parsed by a single-node decision tree algorithm

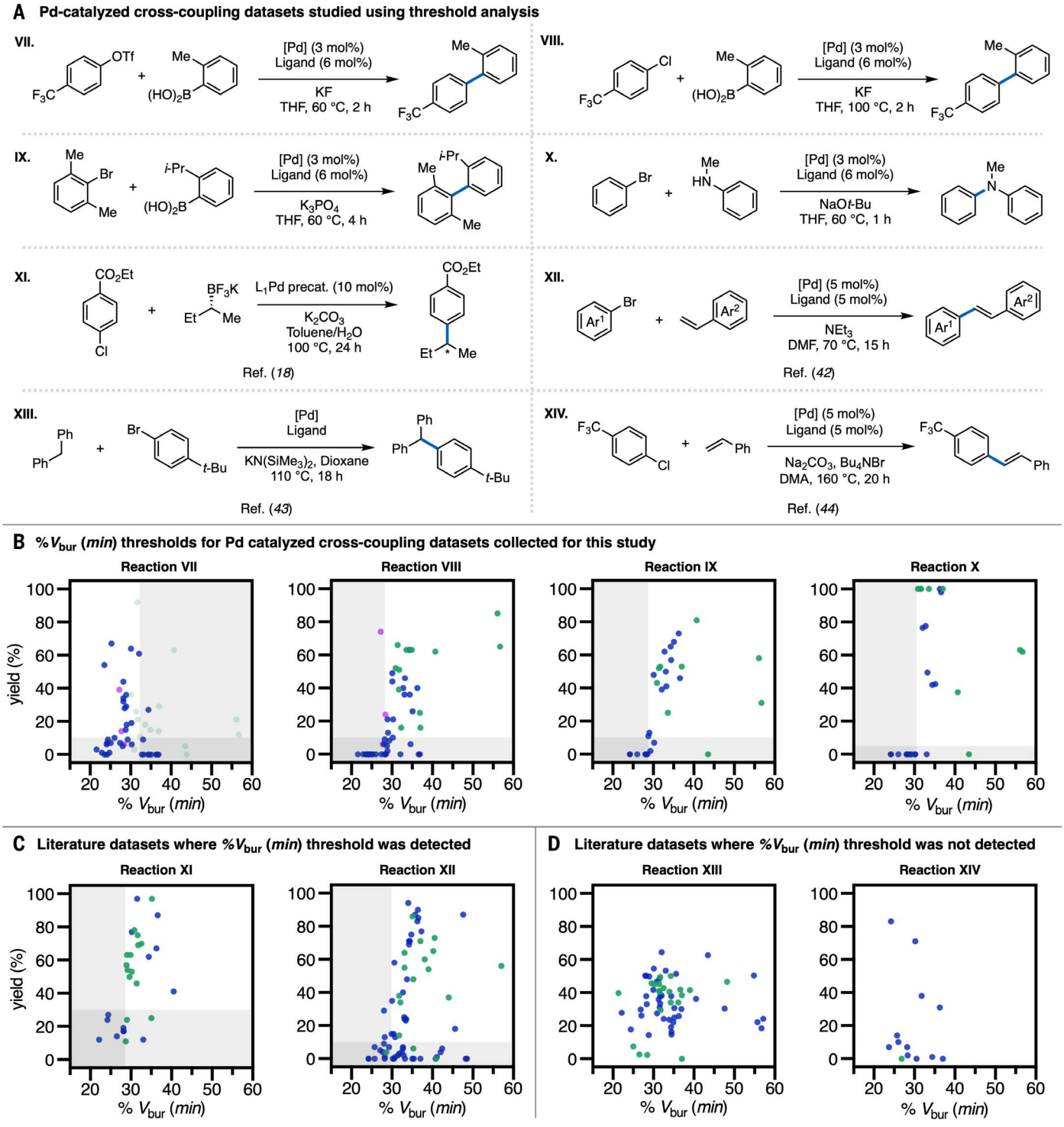

Fig. 5. Threshold analysis for Pd-catalyzed cross-coupling reactions. (**A**) Reaction schemes for the reactions analyzed. Reactions VII to X were collected for this study (see SM for exact reaction conditions), and reactions XI (*18*), XII (*42*), XIII (*43*), and XIV (*44*) were mined from literature sources. Ar, aromatic ring. (**B**) Threshold analysis of Pd datasets for reactions VII to X. (**C**) Threshold analysis of literature Pd datasets for reactions XI and XII. (**D**) Threshold analysis of literature Pd datasets for reactions XIII and XIV, where no $\%V_{bur}$ (min) threshold is present. For all plots, pink dots represent DinoPhos-type ligands, green dots represent Buchwald-type ligands, and blue dots represent all others.

equipped with any descriptor sets provided to it. The algorithm then determines the location of the threshold (if present) for each descriptor, along with statistical measures to assess the quality of the binary classification (see SM for details). A consequence of this analysis is the dissection of datasets into four quadrants of a confusion matrix: (i) active ligands that meet the threshold ligation state criterion (true positives), (ii) inactive ligands that correctly do not meet the criterion (true negatives), (iii) active ligands that do not meet the criterion (false negatives), and (iv) inactive ligands that meet the criterion but fail for other reasons (false positives) (*36*). These groupings can then be analyzed further using statistical modeling or as targets for mechanistic interrogation (*37*).

Applying this workflow to the Ni datasets, we were able to evaluate the algorithm's ability to computationally identify and quantify the thresholds initially observed for these reactions (see SM and tables S11 and S12 for details). Most of the false positives in the classifications were ligands that were either electron-poor or contained catalyst-poisoning functionality and thus failed for reasons other than ligation state. As an example, P(4-CF_3Ph)$_3$ was found to form L_2Ni(4-fluorobenzaldehyde) complexes but was inactive in all of the catalytic reactions.

Threshold analysis in Pd-catalyzed cross-coupling reactions

Considering the success of the classification tool for Ni-catalyzed cross-coupling reactions, we sought to determine if %V_{bur} (min) could also be applied in identifying reactivity thresholds more broadly. In particular, we investigated various Pd-catalyzed cross-coupling reactions wherein the formation of L_1Pd versus L_2Pd species has been demonstrated to be a key factor in determining reaction outcome (*26*, *38*). In one case study, we probed a Pd-catalyzed SMC of aryl triflates, for which L_2Pd is proposed to be necessary for C–O bond oxidative addition (reaction VII; Fig. 5A) (*26*, *39*). The requirement for L_2Pd in catalysis also provided an opportunity to test the DinoPhos ligands for the first time in Pd catalysis. We generated a dataset using 56 phosphines and found a %V_{bur} (min) reactivity threshold at 32.4% (reaction VII; Fig. 5B). The reactivity cliff mirrored those of the Ni systems in both the cutoff value and directionality of active and inactive regions. Further, DrewPhos and CyTyrannoPhos were both correctly classified as active ligands based on their %V_{bur} (min) values below the threshold and performed similarly to "undecorated" PPh_3 and $CyPPh_2$, respectively. Spectroscopic studies corroborated these results, with the detection of L_2Pd(dba) by ^{31}P NMR for DrewPhos and the DinoPhos ligands studied, including the less active CyTriceraPhos (dba, dibenzylideneacetone; figs. S97 to S101). A necessity of the analysis for reaction VII was to partition and classify Buchwald-type phosphines separately, regardless of %V_{bur} (min) (see SM for details). This is likely a result of their ability to occupy two coordination sites, a design element of these ligands that allows them to mimic an L_2Pd species during catalysis through stabilizing Pd-arene interactions (*23*, *39*, *40*). Consistent with previous investigations by the Sigman lab into the chemoselectivity of aryl triflate SMCs (*39*), P(*o*-tolyl)$_3$ was an outlier in the reaction, despite likely favoring L_1Pd species under the reaction conditions (*41*).

In the next set of case studies, various reactions where L_1Pd species are implicated were evaluated with the classification workflow. We generated datasets for two Pd-catalyzed SMCs (reactions VIII and IX; Fig. 5A) with aryl halides, including one reaction with sterically hindered coupling partners, as well as a dataset for a Buchwald-Hartwig amination (reaction X; Fig. 5A). For the two SMCs, the classification tool revealed a threshold at about 29% V_{bur} (min), with the active region occurring above that value, indicating that larger ligands—as defined by %V_{bur} (min)—are required for effective catalysis (reactions VIII and IX; Fig. 5B). When comparing reactions VII and VIII**,** the opposite directionalities of the observed thresholds are consistent with the extensive literature precedent studying the effects of ligation state on the chemoselectivity of aryl triflate versus aryl chloride bond activation (*26*, *38*, *39*). Perhaps the most pronounced example is that of the Buchwald-Hartwig amination (reaction X; Fig. 5B) with a clear reactivity cliff between high-yielding reactions and those with 0% yield at and below 31% V_{bur} (min). Two datasets mined from the literature were also evaluated: a stereospecific Pd-catalyzed SMC previously studied by Biscoe, Sigman, and co-workers (*18*) (reaction XI; Fig. 5A) and a Heck reaction reported by Hartwig and co-workers (*42*) (reaction XII; Fig. 5A). In both cases, %V_{bur} (min) thresholds were observed and suggest that L_1Pd species are responsible for catalysis (reactions XI and XII; Fig. 5B).

We recognized that there are circumstances where ligand steric properties may not have as great of an impact on the reaction outcome, and thus a threshold would not be expected. In our literature-mining efforts, we identified two datasets where no phosphine steric threshold was found: a Pd-catalyzed Csp^3–H arylation reported by Dreher, Walsh, and co-workers (*43*) (reaction XIII; Fig. 5) and a Pd-catalyzed Heck cross-coupling studied by Zapf and Beller (*44*) (reaction XIV; Fig. 5). Possible explanations for these examples include high levels of ligandless background reactivity and/or catalytic cycles that are less sensitive to ligation state, possibly owing to the generation of catalytically active Pd nanoparticles (*45*, *46*). The ability to rapidly identify these scenarios in datasets can serve as a valuable mechanistic probe given the physical significance of %V_{bur} (min) (vide supra).

Summary and outlook

The threshold values and directionality found for each of the datasets studied in this work are summarized in Fig. 6. Comparing the Ni- and Pd-catalyzed reactions reveals several mechanistically interesting features about Ni and Pd catalysis, as well as phosphine steric effects more generally. First, the opposite threshold directionalities of the Ni- and Pd-catalyzed SMC reactions of aryl halides (reactions II to V, VIII, and IX) point to different ligation state requirements between the two metals for this reaction (*47*). Thus, the classification workflow provides a means to compare Ni and Pd head to head and elucidates the orthogonal ligand design principles often necessary for each metal (*19*, *48*).

Second, the location of the threshold for the Ni and Pd datasets occurs with some variation in value. However, for all of the reactions tested (with the exception of reaction X), an overlap area can be observed wherein ligands with %V_{bur} (min) values between 29 and 32% work, independent of the directionality of the threshold. This may signify a region of %V_{bur} (min) values in which L_2M is thermodynamically favored in the resting state but L_1M is also present in solution; within this region, the equilibrium between L_2M and L_1M would be affected by the temperature, solvent, and concentration of the reaction. This is known to be the case with phosphines such as PCy_3 (*38*), and the decrease in ΔG_{dissoc} between 29 and 32% (Fig. 4C) corroborates this hypothesis. Even in the data for Ni-catalyzed cross-couplings, the most active ligands generally fell within these limits (Fig. 2). This observation suggests that L_1 intermediates and/or transition states

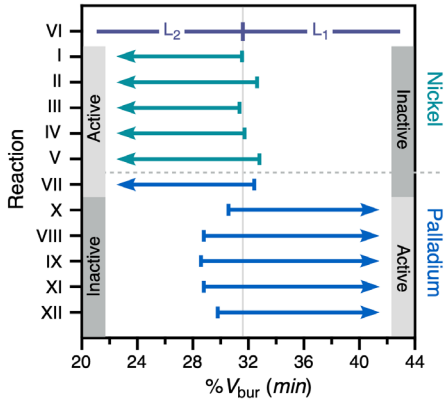

Fig. 6. Summary of reactivity thresholds. %V_{bur} (min) reactivity threshold locations and directionalities for all Ni-catalyzed [reactions I to V (green)] and Pd-catalyzed [reactions VII to XII (blue)] reactions under study (excluding reactions XIII and VIV, where no threshold was found). The L_1 and L_2 regions defined by the spectroscopic ligation state studies are shown [reaction VI (purple)].

may be relevant in Ni catalysis (*49*, *50*) but that the ability to attain an L_2 resting state is necessary (*32*, *51*, *52*), as evidenced by the sharp reactivity cliffs.

We have developed a strategy for the binary classification of monodentate phosphine ligation state and reactivity in cross-coupling catalysis. In searching the feature space of structurally diverse monodentate phosphines, we identified $\%V_{bur}$ (min) as the descriptor capable of bifurcating datasets on the basis of catalyst ligation state. We envision that this tool should facilitate mechanistic studies of related organometallic reactions and enable reaction development through prediction of active and inactive and mono- and bis-ligating phosphines before synthesis. Though we recognize that $\%V_{bur}$ (min) will not capture reactivity trends across all phosphines, the ability to identify outliers (especially false negatives) in the analysis can motivate the development of new descriptors and targeted mechanistic study. Taken together, this study highlights how classification analysis can serve as an important mechanistic and predictive tool to facilitate the understanding of structure-reactivity relationships in catalysis.

REFERENCES AND NOTES

1. E. V. Anslyn, D. A. Dougherty, *Modern Physical Organic Chemistry* (Univ. Science Books, 2006).
2. C. B. Santiago, J. Y. Guo, M. S. Sigman, *Chem. Sci.* **9**, 2398–2412 (2018).
3. L. P. Hammett, *J. Am. Chem. Soc.* **59**, 96–103 (1937).
4. P. R. Wells, *Chem. Rev.* **63**, 171–219 (1963).
5. N. A. Romero, D. A. Nicewicz, *Chem. Rev.* **116**, 10075–10166 (2016).
6. D. G. Brown, J. Boström, *J. Med. Chem.* **59**, 4443–4458 (2016).
7. S. Xu, E. H. Kim, A. Wei, E. I. Negishi, *Sci. Technol. Adv. Mater.* **15**, 044201 (2014).
8. J. F. Hartwig, *Organotransition Metal Chemistry: From Bonding to Catalysis* (Univ. Science Books, 2010).
9. C. C. C. Johansson Seechurn, M. O. Kitching, T. J. Colacot, V. Snieckus, *Angew. Chem. Int. Ed.* **51**, 5062–5085 (2012).
10. D. J. Durand, N. Fey, *Chem. Rev.* **119**, 6561–6594 (2019).
11. C. A. Tolman, *J. Am. Chem. Soc.* **92**, 2956–2965 (1970).
12. C. A. Tolman, *Chem. Rev.* **77**, 313–348 (1977).
13. D. White, B. C. Tavener, P. G. L. Leach, N. J. Coville, *J. Organomet. Chem.* **478**, 205–211 (1994).
14. K. C. Harper, E. N. Bess, M. S. Sigman, *Nat. Chem.* **4**, 366–374 (2012).
15. A. Poater *et al*., *Eur. J. Inorg. Chem.* **2009**, 1759–1766 (2009).
16. H. Clavier, S. P. Nolan, *Chem. Commun.* **46**, 841–861 (2010).
17. L. Falivene *et al*., *Nat. Chem.* **11**, 872–879 (2019).
18. S. Zhao *et al*., *Science* **362**, 670–674 (2018).
19. K. Wu, A. G. Doyle, *Nat. Chem.* **9**, 779–784 (2017).
20. H. Y. Liu, K. Eriks, A. Prock, W. P. Giering, *Organometallics* **9**, 1758–1766 (1990).
21. T. Gensch *et al*., ChemRxiv 12996665 [Preprint] (2021); http://doi.org/10.26434/chemrxiv.12996665.v1.
22. F. Barrios-Landeros, B. P. Carrow, J. F. Hartwig, *J. Am. Chem. Soc.* **131**, 8141–8154 (2009).
23. R. Martin, S. L. Buchwald, *Acc. Chem. Res.* **41**, 1461–1473 (2008).
24. A. A. Thomas, A. F. Zahrt, C. P. Delaney, S. E. Denmark, *J. Am. Chem. Soc.* **140**, 4401–4416 (2018).
25. G. C. Fu, *Acc. Chem. Res.* **41**, 1555–1564 (2008).
26. F. Schoenebeck, K. N. Houk, *J. Am. Chem. Soc.* **132**, 2496–2497 (2010).
27. T. Gensch *et al*., ChemRxiv chemrxiv-2021-fgm7v [Preprint] (2021); http://doi.org/10.33774/chemrxiv-2021-fgm7v.
28. A. P. Cinderella, B. Vulovic, D. A. Watson, *J. Am. Chem. Soc.* **139**, 7741–7744 (2017).
29. Cone angle values used in the text are those for the Boltzmann weighted average of the conformational ensemble from the descriptor library. Minimum cone angles were also evaluated but for simplicity are shown in fig. S2.
30. A. J. Kendall, L. N. Zakharov, D. R. Tyler, *Inorg. Chem.* **55**, 3079–3090 (2016).
31. Buchwald-type phosphines are known to act as structurally bidentate-like ligands with Pd owing to stabilizing interactions between the arene and the metal. Although little is known as of now about the structural behavior of these ligands with Ni, this semibidentate binding may enable certain Ni-catalyzed reactions to occur despite only one phosphine bound; their mode of action in these case studies is the subject of ongoing investigation.
32. E. A. Standley, S. J. Smith, P. Müller, T. F. Jamison, *Organometallics* **33**, 2012–2018 (2014).
33. D. Walther, *J. Organomet. Chem.* **190**, 393–401 (1980).
34. M. Ohashi, H. Saijo, T. Arai, S. Ogoshi, *Organometallics* **29**, 6534–6540 (2010).
35. I. A. Guzei, M. Wendt, *Dalton Trans.* **2006**, 3991–3999 (2006).
36. Given that other ligand features can and will lead to poor catalyst performance, the presence of false positives should not be viewed as detrimental to the success and/or accuracy of the classifier.
37. Z. L. Niemeyer *et al*., *J. Am. Chem. Soc.* **139**, 12943–12946 (2017).
38. A. F. Littke, C. Dai, G. C. Fu, *J. Am. Chem. Soc.* **122**, 4020–4028 (2000).
39. Z. L. Niemeyer, A. Milo, D. P. Hickey, M. S. Sigman, *Nat. Chem.* **8**, 610–617 (2016).
40. K. L. Billingsley, K. W. Anderson, S. L. Buchwald, *Angew. Chem. Int. Ed.* **45**, 3484–3488 (2006).
41. J. F. Hartwig, F. Paul, *J. Am. Chem. Soc.* **117**, 5373–5374 (1995).
42. J. P. Stambuli, S. R. Stauffer, K. H. Shaughnessy, J. F. Hartwig, *J. Am. Chem. Soc.* **123**, 2677–2678 (2001).
43. J. Zhang, A. Bellomo, A. D. Creamer, S. D. Dreher, P. J. Walsh, *J. Am. Chem. Soc.* **134**, 13765–13772 (2012).
44. A. Zapf, M. Beller, *Chemistry* **7**, 2908–2915 (2001).
45. S. S. Zalesskiy, V. P. Ananikov, *Organometallics* **31**, 2302–2309 (2012).
46. N. W. J. Scott *et al*., *Chem. Sci.* **10**, 7898–7906 (2019).
47. S. Z. Tasker, E. A. Standley, T. F. Jamison, *Nature* **509**, 299–309 (2014).
48. C. M. Lavoie, M. Stradiotto, *ACS Catal.* **8**, 7228–7250 (2018).
49. H. Shirataki, M. Ohashi, S. Ogoshi, *Eur. J. Org. Chem.* **2019**, 1883–1887 (2019).
50. We recognize that there are some instances where Ni will be L_1 throughout the catalytic cycle, allowing ligands like P(*t*-Bu)$_3$ to be used successfully; see (*49*).
51. N. Hazari, P. R. Melvin, M. M. Beromi, *Nat. Rev. Chem.* **1**, 0025 (2017).
52. P.-A. Payard, L. A. Perego, I. Ciofini, L. Grimaud, *ACS Catal.* **8**, 4812–4823 (2018).
53. E. Peters, SigmanGroup/threshold: Single parameter threshold (1.0.0). Zenodo (2021); http://doi.org/10.5281/zenodo.5227162.

ACKNOWLEDGMENTS

We thank P. Jeffrey for assistance with x-ray structure determination and K. Wu for helpful discussions and directions. Additionally, we thank F. D. Toste for helpful discussions related to the preparation of the manuscript. **Funding:** NSF CCI Center for Computer Assisted Synthesis (CHE-1925607). **Author contributions:** T.G., M.S.S., and A.G.D. conceived the project. S.H.N.-S., S.R.S., J.E.B., and H.C.J. performed the experiments and analyzed the data. E.P., T.G., and S.R.S. developed the classification algorithm. M.S.S. and A.G.D. oversaw the project. S.H.N.-S., J.E.B., S.R.S., M.S.S., and A.G.D. wrote the manuscript with contributions from all authors. **Competing interests:** The authors declare no competing interests. **Data and materials availability:** X-ray crystallographic data are available free of charge from the Cambridge Crystallographic Data Centre, under reference numbers 2069892 to 2069895. Coordinates of all computed structures are included in a separate zip file. All other experimental, computational, spectroscopic, and crystallographic data are included in the supplementary materials. The code used in this project is available at https://github.com/sigmangroup/threshold (*53*).

SUPPLEMENTARY MATERIALS

science.org/doi/10.1126/science.abj4213
Materials and Methods
Figs. S1 to S121
Tables S1 to S30
References (*54*–*95*)
Data S1

11 May 2021; accepted 2 September 2021
10.1126/science.abj4213

Univariate classification of phosphine ligation state and reactivity in cross-coupling catalysis

Samuel H. Newman-StonebrakerSleight R. SmithJulia E. BorowskiEllyn PetersTobias GenschHeather C. JohnsonMatthew S. SigmanAbigail G. Doyle

Science, 374 (6565), • DOI: 10.1126/science.abj4213

Which phosphines squeeze together?

Phosphine ligands coordinated to palladium and nickel are essential tools for assembling the backbones of pharmaceutical compounds. For decades, descriptors that characterize spatial bulk have helped to guide phosphine optimization. However, these descriptors tend to apply to ideal geometries of a single ligand. Newman-Stonebraker *et al*. introduce a descriptor that considers how the ligand conformation might change in a crowded environment. Specifically, they found that the minimum percentage buried volume accurately predicts when one or two of a particular ligand will coordinate to a metal center, frequently a key determinant of successful catalysis. —JSY